Quantum state-to-state cross sections for atom-diatom reactions: A Chebyshev real wave-packet approach

Shi Ying Lin and Hua Guo*
Department of Chemistry, University of New Mexico, Albuquerque, New Mexico 87131, USA
(Received 24 May 2006; published 1 August 2006)

We describe the implementation of a quantum mechanical method to calculate state-to-state differential cross sections for atom-diatom reactive scattering processes. The key ingredient of this approach is the efficient and accurate propagation of a real scattering wave packet in the Chebyshev order domain, from which the *S*-matrix elements can be extracted. This approach is implemented with Open MP and applied to compute differential and integral cross sections for the direct $H+H_2$ abstraction reaction and the more challenging $N(^2D)+H_2$ insertion reaction.

DOI: 10.1103/PhysRevA.74.022703 PACS number(s): 34.50.Lf, 34.50.Pi

I. INTRODUCTION

Recent advances in crossed molecular beam experiments have allowed the interrogation of several gas phase elementary reactions with an unprecedented level of detail [1–4]. The progress can be largely attributed to novel detection techniques that have greatly improved the capability and sensitivity in measuring the most detailed scattering attributes, namely, the differential cross sections (DCSs). Indeed, the fully quantum state resolved product angular distributions have revealed many intricate and surprising features of reactive scattering. For instance, forward scattering in the direct hydrogen exchange ($H+H_2$) reaction has recently been observed and interpreted as the result of threshold effects near the barrier [5–7]. The signature of Feshbach resonances in the DCS has also been detected recently for the $F+H_2$ reaction [8]. Such quantum state resolved information sheds much light on reactive scattering processes, especially with a direct and detailed comparison with quantum mechanics.

Although the full-dimensional quantum mechanical theory for atom-diatom (e.g., $H+H_2$) scattering processes was established in 1970s [9], converged state-to-state quantum DCSs are still uncommon today and mostly restricted to light systems and low collision energies. There are two major approaches to the exact quantum mechanical calculation of *S*-matrix elements for reactive scattering processes [10–12]. The time-independent approach solves either coupled-channel (CC) [13] or variationally derived algebraic equations [14], and yields the entire *S* matrix at a given energy. This approach, as exemplified by the popular *ABC* code [15], is an accurate, robust, and mature method and has been used to generate DCSs for several atom-diatom problems. However, it requires a large core memory and the number of arithmetic operations scales steeply with the number of channels in the system. Hence, its further applications to heavier and/or larger systems are severely limited.

On the other hand, the time-dependent approach extracts scattering information from a wave packet [16–19]. The wave-packet approach is ideally suited for studying initial state specified scattering processes since the initial wave packet corresponds to a well-defined reactant state. Unlike the CC approach, each propagation yields a column of the *S* matrix, but in a range of energies. The variation of DCSs with the collision energy is particularly important for understanding the role played by various resonances [3,4,20]. Although the majority of wave-packet studies of reactive scattering have so far been devoted to the calculation of total or state-resolved reaction probabilities, there is no reason why such an approach cannot be used to compute the transition amplitudes [21], which are needed to construct DCSs. Indeed, successful applications of the wave-packet approach in calculating DCSs have recently been demonstrated [22,23]. Numerically, the wave-packet approach has much more favorable scaling laws than the CC approach in both memory and number of arithmetic operations, thus rendering it amenable to heavier atom-diatom processes and reactive systems with more than three atoms. Understandably, the wave-packet approach is best suited for fast reactions, but as shown in this work it is also applicable to complex-forming reactions.

In this paper, we discuss the implementation of an efficient and accurate wave-packet method for calculating *S*-matrix elements and thus DCSs for atom-diatom reactive scattering. The key ingredient of this approach is the propagation of the scattering wave packet in the Chebyshev order domain, which is more accurate and efficient than that in the time domain. The *S*-matrix elements in the energy domain are obtained from a discrete Fourier transform of cross-correlation functions. First introduced by Kosloff and co-workers [24,25] and by Kouri and co-workers [26–29], the Chebyshev propagation bears many similarities with time propagation. Indeed, it has been pointed out that the Chebyshev operator is a discrete cosine evolution operator [30,31]. As a result, methods developed for the time-dependent wave packet can be readily transplanted to the Chebyshev wave packet. The applicability of this approach in calculating state-resolved and total transition probabilities in inelastic and reactive scattering has recently been demonstrated by us [32–35]. We note in passing that our method shares essentially the same propagation scheme with the recent work of Gray and Balint-Kurti [31], and of Althorpe and co-workers [22,36,37], but it differs with them in many other aspects.

*Corresponding author; FAX: 505 277 2609. Electronic address: hguo@unm.edu

This paper is organized as follows. The next section (Sec. II) outlines the theoretical details, including the discretization and propagation of the scattering wave packet and the extraction of the S-matrix elements and differential and integral cross sections. The results are presented in Sec. III, followed by conclusions (Sec. IV).

II. THEORY

A. Hamiltonian and discretization

For $A+BC \rightarrow AB+C$ reactions, we employed the product Jacobi coordinates (R,r,γ) where r and R are, respectively, the bond length of the product diatom (A-B) and the distance between the atom (C) and the center of mass of the diatom (AB), and γ is the enclosed angle. This choice is convenient for calculating state-to-state scattering attributes in the product channel. In these coordinates, the Hamiltonian is expressed as ($\hbar=1$)

$$\hat{H} = -\frac{1}{2\mu_R}\frac{\partial^2}{\partial R^2} - \frac{1}{2\mu_r}\frac{\partial^2}{\partial r^2} + \frac{\hat{j}^2}{2\mu_r r^2} + \frac{\hat{l}^2}{2\mu_R R^2} + V(R,r,\gamma), \tag{1}$$

where μ_r and μ_R are the corresponding reduced masses for the radial Jacobi coordinates, and $V(R,r,\gamma)$ is the potential energy surface. $\hat{l}^2$, the square of the orbital angular momentum operator, can be further expressed as

$$\hat{l}^2 \equiv (\hat{J}-\hat{j})^2 = \hat{J}^2 + \hat{j}^2 - 2\hat{J}_z\hat{j}_z - \hat{J}_+\hat{j}_- - \hat{J}_-\hat{j}_+, \tag{2}$$

in which $\hat{J}$ and $\hat{j}$ are, respectively, the total and diatomic angular momentum operators with $\hat{J}_z$ and $\hat{j}_z$ as their projections onto the body-fixed (BF) z axis, namely the R vector. $\hat{J}_+$ ($\hat{J}_-$) and $\hat{j}_+$ ($\hat{j}_-$) are the corresponding raising (lowering) operators.

Following our earlier work [34], the Hamiltonian and wave packet were discretized in a mixed discretized representation, consisting of a direct product discrete variable representation [38] for the two radial degrees of freedom and a finite basis representation (FBR) for the angular degrees of freedom. In particular, a wave packet with a total angular momentum J and parity p is expressed as

$$|\psi^{Jp}\rangle = \sum_{\alpha_1\alpha_2 j\Omega} \psi^{Jp}_{\alpha_1\alpha_2 j\Omega}|\alpha_1\alpha_2\rangle|j\Omega;Jp\rangle, \tag{3}$$

where α_1 and α_2 denote the indices of the equidistant Fourier R and r grids, respectively. The actions of the radial kinetic energy operators (KEOs) onto the wave packet can be efficiently calculated using the fast sine-Fourier transform method [39].

The parity-adapted angular basis is defined below:

$$|j\Omega;Jp\rangle = (2+2\delta_{\Omega,0})^{-1/2}[|J\Omega\rangle|j\Omega\rangle + p(-1)^J|J-\Omega\rangle|j-\Omega\rangle], \tag{4}$$

where $|j\Omega\rangle \equiv \Theta_{j\Omega}(\gamma,0)$ are normalized associate Legendre functions with the Condon-Shortley phase convention [40], and $|J\Omega\rangle = \sqrt{(2J+1)/8\pi^2}D^{J*}_{\Omega,0}$ represents the overall rotation, where $D^J_{\Omega,M}$ is the Wigner rotation matrix [41]. The projection of J and j onto the z axis in the BF frame, Ω, is thus restricted to be non-negative. In this basis, all rotational KEOs in Eq. (1) are diagonal except the Coriolis coupling term which is tridiagonal. In particular,

$$\langle j'\Omega';Jp|\hat{j}^2|j\Omega;Jp\rangle = j(j+1)\delta_{j',j}\delta_{\Omega',\Omega}, \tag{5a}$$

$$\begin{aligned}\langle j'\Omega';Jp|\hat{l}^2|j\Omega;Jp\rangle &= [J(J+1)+j(j+1)-2\Omega^2]\delta_{j',j}\delta_{\Omega',\Omega} - [(1+\delta_{\Omega',0})\\ &\times(1+\delta_{\Omega,0})]^{-1/2}\{\lambda^+_{J\Omega}\lambda^+_{j\Omega}\delta_{\Omega',\Omega+1} + \lambda^-_{J\Omega}\lambda^-_{J\Omega}\\ &\times[\delta_{\Omega',\Omega-1} + p(-1)^J\delta_{\Omega',-\Omega+1}]\}\delta_{j',j},\end{aligned} \tag{5b}$$

where $\lambda^{\pm}_{jm} = \sqrt{j(j+1)-m(m\pm1)}$. Because Ω and Ω' are restricted to non-negative values, the last term in Eq. (5b) survives only for $\Omega=0,1$.

The use of FBR simplifies the rotational KEOs, but complicates the calculation of the action of potential energy operator. To solve this problem, the following pseudo-spectral transformation was used to convert the wave packet from the angular FBR to a grid [42,43]:

$$T^{(\Omega)}_{j\beta} = \sqrt{w_\beta}\Theta_{j\Omega}(\gamma_\beta), \tag{6}$$

where β denotes the index of the Gauss-Legendre quadrature points for the internal (Jacobi) angular coordinate and w_β is the corresponding weight.

For insertion reactions, the wave packet can easily access regions near $R=0$. Even without the explicit inclusion of the singularity, it may result in a very large spectral range. To alleviate this problem, we used a scheme to restrict the spectral range of the rotational KEOs at small R. In particular, the BF-FBR $|j\Omega;Jp\rangle$ is first transformed to the SF-FBR $|jl;Jp\rangle$ using the following formula [41,44]:

$$|j\Omega;Jp\rangle = \sum_l (-1)^{j-l+\Omega}\sqrt{(2-\delta_{\Omega,0})(2l+1)}\begin{pmatrix} j & l & J \\ \Omega & 0 & -\Omega \end{pmatrix} \times|jl;Jp\rangle, \tag{7}$$

where $(:::)$ denotes the 3-j symbol [41]. Because the rotational KEOs are all diagonal in the SF-FBR, the spectral range can be easily controlled by truncating the rotational energy. After applying the truncated rotational KEOs, the wave function is transformed back to the original BF-FBR. The drawback of this method is that computationally it is slightly more expensive to compute the matrix-vector multiplication.

B. Chebyshev propagation

As described below, the S-matrix elements can be extracted from the scattering wave packet propagated in the Chebyshev order domain. Starting from an initial wave packet, the Chebyshev propagation is carried out using the following modified Chebyshev recursion relationship proposed by Mandelshtam and Taylor [45,46]:

$$|\psi_{k+1}\rangle = D(2\hat{H}_{scaled}|\psi_k\rangle - D|\psi_{k-1}\rangle) \tag{8}$$

with $|\psi_1\rangle = D\hat{H}_{scaled}|\psi_0\rangle$ and $|\psi_0\rangle = |\chi_i\rangle$. The damping function D is applied at the grid edges. In this work, the following Gaussian shaped damping function was used:

$$D(R) = \begin{cases} 1 & \text{for } x \le x_d \\ e^{-d_x(x-x_d)^2} & \text{for } x > x_d \end{cases} \quad (x = R, r). \tag{9}$$

The damping is equivalent to the negative imaginary potential [47] used in the time propagation to enforce the outgoing boundary conditions.

To maintain stability of the propagation, the Hamiltonian has to be properly scaled

$$\hat{H}_{scaled} = (\hat{H} - H^+)/H^- \tag{10}$$

to avoid the divergence of the Chebyshev polynomials outside the range $[-1,1]$. Here, the spectral medium and half-width of the Hamiltonian $H^{\pm} = (H_{\max} \pm H_{\min})/2$ are calculated from the spectral extrema, $H_{\max}$ and $H_{\min}$, which can be readily estimated [24].

Although the Chebyshev polynomials have long been used as building blocks in approximating operator functions [24,28,29], it has recently been realized that they themselves can also be regarded as a discrete cosine evolution operator with a mapped Hamiltonian: $T_k(\hat{H}) = \cos(k \arccos \hat{H})$, in which the Chebyshev order k can be considered as generalized time [30,31]. As a result, algorithms designed for the time propagator $(e^{-i\hat{H}t})$ can be readily transplanted to the Chebyshev order domain [48]. The Chebyshev propagation has several advantages over time propagation. First, it can be executed accurately by Eq. (8) while the exponential time propagator has to be approximated. Second, the entire propagation can be carried out in real algebra, provided the initial wave packet is real and the Hamiltonian is discretized with real basis functions [31]. This is also true for systems in the continuum, thanks to the damping scheme in Eq. (8). Third, the nonlinear mapping between energy and the Chebyshev angle $(\vartheta = \arccos E)$ allows a much denser interpolation grid near the spectral extrema, which accelerates the convergence in computing attributes in these regions [49]. Numerically, the memory scales linearly with the dimension of the wave packet since only two vectors need be stored. The matrix-vector multiplication in Eq. (8) scales pseudolinearly with the dimensionality as well because the Hamiltonian matrix is not stored and its action onto the recurring vector is computed using a partial sum method [50].

C. *S* matrix and cross sections

The S-matrix element for a transition from an initial reactant state (i) to a final product state (f) is given by [51,52]

$$S^{Jp}_{f\leftarrow i}(E) = \frac{i\langle\chi_f|G^+(E)|\chi_i\rangle}{2\pi a_i(E)a_f^*(E)}, \tag{11}$$

where a_i and a_f are the energy amplitudes of the reactant and product wave packets (χ_i and χ_f). The casual Green operator can be expressed as the following Chebyshev expansion [25,28,29]:

$$G^+(E) = \frac{1}{E - \hat{H} + i\epsilon} = \frac{-i}{H^-\sqrt{1 - E^2_{scaled}}} \sum_{k=0} (2 - \delta_{k0}) e^{-ik \arccos E_{scaled}} T_k(\hat{H}_{scaled}), \tag{12}$$

where the energy is similarly scaled as in Eq. (10): $E_{scaled} = (E - H^+)/H^-$. The infinitesimal number ϵ in $G^+(E)$ can be interpreted as the absorbing boundary conditions [53], and implemented by the damping scheme in Eq. (8).

Substituting Eq. (12) back to Eq. (11), the S-matrix element is expressed as a discrete Fourier transform of the cross-correlation functions, $C_k^{(f\leftarrow i)} \equiv \langle\chi_f|\psi_k\rangle$:

$$S^{Jp}_{f\leftarrow i}(E) = \frac{1}{2\pi H^- \sin\vartheta a_i(E)a_f^*(E)} \sum_{k=0} (2 - \delta_{k,0}) e^{-ik\vartheta} C_k^{(f\leftarrow i)}, \tag{13}$$

where the Chebyshev angle is given by $\vartheta = \arccos E_{scaled}$ and the Chebyshev wave packet $|\psi_k\rangle = T_k(\hat{H}_{scaled})|\psi_0\rangle$ was propagated by the modified three-term Chebyshev recursion relationship in Eq. (8). The scalar correlation functions were calculated along the propagation and stored.

The initial wave packet $|\psi_0\rangle = |\chi_i\rangle$, which is by definition localized in the asymptotic reactant region, can be chosen as a product of a well-defined rovibrational eigenfunction $|\varphi_{v_i j_i}\rangle$ of the diatomic molecule BC, a space-fixed angular momentum eigenstate in the coupled representation ($|JMj_il_i\rangle$), and a one-dimensional Gaussian-shaped wave packet along the A-BC translational coordinate. In particular, the following form in the reactant Jacobi coordinates (R', r', γ') was used:

$$|\psi_0\rangle = Ne^{-(R' - R'_0)^2/2\delta^2} \cos k_0 R' |\varphi_{v_i j_i}\rangle |JMj_il_i\rangle, \tag{14}$$

where k_0, R'_0, and δ are its mean momentum, position, and width, respectively, and N is the normalization constant. v_i and j_i stand for the vibrational and rotational quantum numbers of a reactant diatomic molecule (BC), respectively. The initial orbital angular momentum l_i is allowed to take values between $|J - j_i|$ and $J + j_i$, and M is the projection of J on the space-fixed (SF) z axis. Since the initial wave packet is real, the propagation in Eq. (8) can be carried out entirely with real algebra [31], which represents significant savings over the complex time propagation.

The use of the SF angular momentum eigenstate in the initial wave packet was motivated by the fact that the corresponding long-range centrifugal term $[l(l+1)/2\mu_{R'}R'^2]$ is analytically accounted for by the spherical Bessel/Hankel functions [21,22,44]. As a result, the initial wave packet can be placed at a relatively small R', where the interaction potential starts to vanish. This can also be done in the BF helicity representation, but with more complexity [22].

We chose in this work to propagate the wave packet in the product Jacobi coordinates. Thus, the initial wave packet defined in Eq. (14) needs be transformed before the propaga-

tion. One can, of course, devise various schemes to perform the coordinate transform during the propagation [54,55], but such transformation could be costly and may introduce unnecessary errors. An alternative is to utilize the reactant-product decoupling scheme [22,56–58], which divides the entire system into multiple regions where different coordinates are used.

The choice of the final state wave packet $|\chi_f\rangle$ was similar to that of the initial wave packet, except the Gaussian wave packet was replaced with the Dirac delta function:

$$|\chi_f\rangle = \delta(R - R_\infty)|\varphi_{v_f j_f}\rangle|JMj_f l_f\rangle, \tag{15}$$

where v_f and j_f stand for the vibrational and rotational quantum numbers of the final states, respectively. The rationale for using the SF angular momentum representation is the same for the initial wave packet as discussed above. As a result, R_∞ can be chosen at a point where the interaction potential just becomes zero. The orbital angular momentum l_f is allowed to take values between $|J-j_f|$ and $J+j_f$. Note, however, that the values of l_f are subject to the restriction $(-1)^{(j_i+l_i)}=(-1)^{(j_f+l_f)}$ due to the parity conservation. With this special choice of the final state wave packet, the correlation function in Eq. (13) can be simplified as a two-dimensional integral

$$C_k^{(f\leftarrow i)} = \langle \varphi_{v_f j_f}|\langle JMj_f l_f|\psi_k(R = R_\infty)\rangle. \tag{16}$$

The energy amplitudes of the initial and final state wave packets, $a_i(E)$ and $a_f(E)$, were obtained as follows:

$$a_i(E) = \left\langle i\sqrt{\frac{\mu_{R'}k_i}{2\pi}}R' h_{l_i}^{(2)}(k_i R')|Ne^{-(R'-R_i')^2|2\delta^2}\cos k_i R' \right\rangle \tag{17a}$$

$$a_f(E) = \left\langle \sqrt{\frac{\mu_R k_f}{2\pi}}R h_{l_f}^{(1)}(k_f R)|\,\delta(R - R_\infty)\right\rangle = \sqrt{\frac{\mu_R k_f}{2\pi}}R_\infty h_{l_f}^{(2)}(k_f R_\infty), \tag{17b}$$

where $h_l^{(1,2)}$ are the spherical Hankel function of the first and second kind [59], and $k_i=\sqrt{2\mu_{R'}(E-E_i)}$ and $k_f=\sqrt{2\mu_R(E-E_f)}$ with E as the total energy and E_i and E_f as the rovibrational energies of reactant and product states, respectively.

Replacing the collective index i or f by the corresponding quantum numbers (v,j,l), the state-to-state integral cross section can be expressed as follows:

$$\sigma_{v_f j_f, v_i j_i}(E) = \frac{\pi}{(2j_i+1)k_{v_i j_i}^2}\sum_{J,p,l_i,l_f}(2J+1)|S_{v_f j_f l_f\leftarrow v_i j_i l_i}^{Jp}(E)|^2. \tag{18}$$

To calculate the differential cross section, it is convenient to first transform the above j,l-specified S-matrix elements to the helicity representation which is j,Ω-specified, using the following formula:

$$S_{v_f j_f \Omega_f\leftarrow v_i j_i \Omega_i}^{Jp} = \sum_{l_i l_f}(U_{l_f\Omega_f}^{Jpj_f})^* S_{v_f j_f l_f\leftarrow v_i j_i l_i}^{Jp} U_{l_i\Omega_i}^{Jpj_i}, \tag{19}$$

where the transformation between BF and SF frames is given as follows [14,60]:

$$U_{l\Omega}^{Jpj} = \frac{i^l}{\sqrt{2(1+\delta_{\Omega,0})}}[\langle j\Omega, J-\Omega|l0\rangle + p(-1)^J\langle j-\Omega, J\Omega|l0\rangle]. \tag{20}$$

Here, $\langle\ldots,\ldots|\cdots\rangle$ denotes the Clebsch-Gordan coefficients [41].

Finally, the differential cross section is then given by [14,60]

$$\frac{d\sigma}{d\Omega}(\theta,E) = \frac{1}{8k_{v_i j_i}^2}\frac{1}{(2j+1)}\sum_{\Omega_f\Omega_i}[|f_+(\theta,E)|^2 + |f_-(\theta,E)|^2], \tag{21}$$

where θ is the scattering angle in the SF frame and

$$f_+(\theta,E) = \sum_{Jp}(2J+1)d_{\Omega_f\Omega_i}^J(\pi-\theta)S_{v_f j_f\Omega_f\leftarrow v_i j_i\Omega_i}^{Jp}(E), \tag{22a}$$

$$f_-(\theta,E) = \sum_{Jp}p(2J+1)d_{\Omega_f\Omega_i}^J(\theta)S_{v_f j_f\Omega_f\leftarrow v_i j_i\Omega_i}^{Jp}(E). \tag{22b}$$

The approach outlined above bears many similarities with several existing wave-packet based methods for computing S-matrix elements [21–23,31,44]. However, significant differences exist. For example, our scheme differs from that of Dai and Zhang in the propagator used in the calculation [21]. Despite similarities in using the Chebyshev propagation, on the other hand, Althorpe's scheme [22] is based on propagating a complex wave packet and employed a Gaussian instead of a delta function in the final state projection. He also used the BF helicity representation in defining both the initial and final states, but computed the S matrix in the SF representation. In addition, he took advantage of the reactant-product decoupling scheme.

III. RESULTS AND DISCUSSION

The computational method outlined above was applied to the $H+H_2\rightarrow H_2+H$ and $N(^2D)+H_2\rightarrow NH+H$ reactions. The former is a benchmark system for abstraction reaction and has been subjected to intensive scrutiny recently from both the experimental and theoretical fronts [3,4,12]. Because of the direct nature of this reaction, wave packet approaches are particularly attractive [22]. The latter, on the other hand, is a prototype for insertion reactions, which have attracted increasing attention lately because of the complexity of the reaction dynamics [1,2]. Because of a deep potential well corresponding to the NH_2 species, the reaction is heavily influenced by resonances. The DCSs for this reaction have been calculated recently at three energies using a time-independent method [61–63], and have shown near symmetry in the forward and backward directions. Here, we only

TABLE I. Numerical parameters used in the calculations. Atomic units are used unless otherwise specified.

	$H+H_2$	$N+H_2$
R_{min}	0.5	0.5
R_{max}	10.5	15.0
n_R	53	127
r_{min}	0.5	0.5
r_{max}	10.5	15.0
n_r	47	127
j_{max}	38	99
n_γ	20	100
R_0'	6.0	9.0
$k_0^2/2\mu$	0.7 eV	0.12 eV
δ	0.15	0.15
R_∞	6.0	8.0
d_R	0.01	0.005
R_d	7.5	11.0
d_r	0.01	0.005
r_d	7.5	11.0

discuss preliminary results for the latter reaction, and a full account of the calculation and more results will be published elsewhere.

All calculations were performed on a 16 node shared memory IBM p590 computer with Open MP at the Albuquerque High Performance Computing Center. In particular, the parallelization was implemented in the matrix-vector calculation which is the most time-consuming step of the calculation. Our simple-minded scheme is based on the partial summation and distributed the matrix-vector multiplication in the outer loop. Such an approach is particularly effective with the shared memory architecture, which avoids latency associated with the message passing interface in distributed memory clusters. Near linear scaling was achieved with regard to the number of nodes in the Open MP environment.

A. $H+H_2$ reaction

The BKMP2 potential energy function [64] was used in our study of the $H+H_2$ reaction. To test the accuracy of our wave-packet results, time-independent CC calculations have also been carried out using the *ABC* code [15]. Extensive convergence tests were performed to determine optimal numerical parameters, which are listed in Table I. Thanks to the permutation symmetry, only half of the angular grid or basis was used. The resulting size of the recurring vector is on the order of half a million.

The energy dependence of various state-to-state integral cross sections from the $v_i=j_i=0$ reactant state is compared in Fig. 1 with the CC results. As the figure shows, the agreement between the two numerically different approaches is visually indistinguishable at all the energy points chosen in the CC runs. To test our wave-packet method at a more rigorous level, state-to-state DCSs were calculated and compared in Fig. 2 with the CC results at two selected energies. Despite the rich structures in the product angular distributions, the agreement is again excellent.

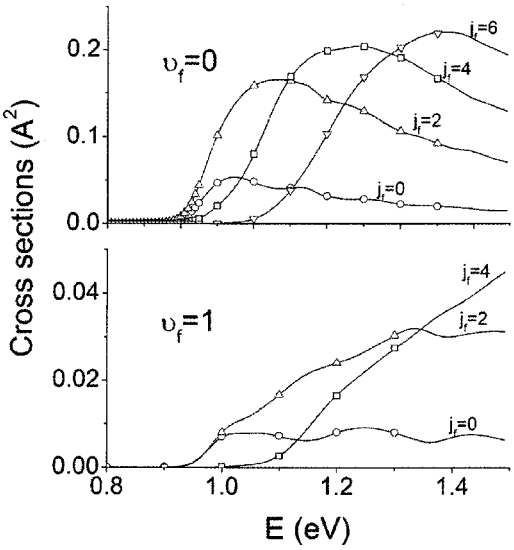

FIG. 1. State-to-state integral cross sections for the $H+H_2(v_i=j_i=0)\rightarrow H+H_2(v_f,j_f)$ reaction. The lines and symbols represent the wave-packet and CC results, respectively.

A distinct feature of the wave-packet approach is that a single propagation yields the scattering attributes in a range of energies. To exploit this trait, we have generated a contour map for the energy dependence of the $00\rightarrow 00$ DCS in Fig. 3. As the figure shows, the angular distribution is broad and dominated by backward scattering at low energies; but with the increase of energy, the forward scattering begins to emerge and sideway scattering diminishes significantly. This is consistent with previous quantum calculations on the same reaction [20,22].

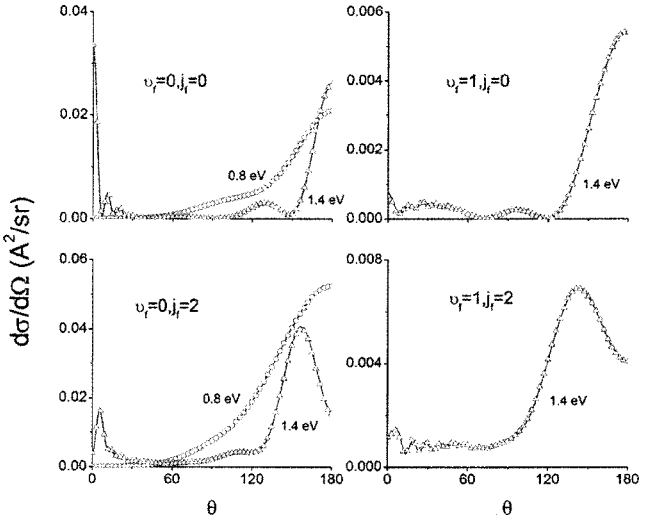

FIG. 2. State-to-state differential cross sections for the $H+H_2(v_i=j_i=0)\rightarrow H+H_2(v_f,j_f)$ reaction at two selected energies. The lines and symbols represent the wave-packet and CC results, respectively.

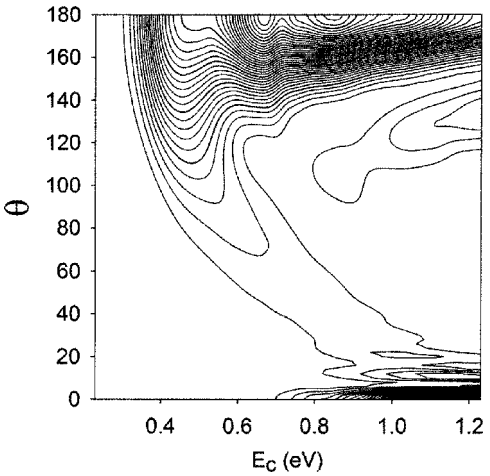

FIG. 3. Energy-angle contour map of the state-to-state differential cross section for the $H+H_2(v_i=j_i=0)\rightarrow H+H_2(v_f=j_f=0)$ reaction calculated with the wave-packet method.

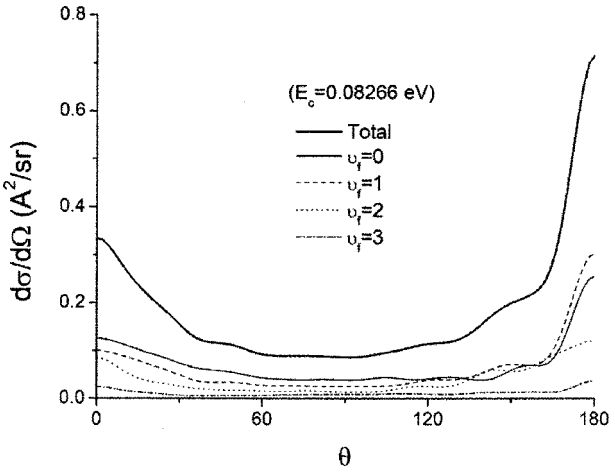

FIG. 4. Vibrational state-resolved and total differential cross sections for the $N+H_2(v_i=j_i=0)\rightarrow NH+H$ reaction at the collision energy of 0.082 66 eV.

All the calculations were obtained with $J_{max}=24$ and all possible values of Ω. Only 1000 steps of the Chebyshev recursion were needed to converge the results. With the same spectral range (H^-), on the other hand, roughly 3000 Chebyshev steps are needed if the wave packet is propagated in time using the Chebyshev interpolation formula of Tal-Ezer and Kosloff [24]. The Chebyshev propagation represents significant savings.

B. $N+H_2$ reaction

The excellent agreement between our wave-packet method and the more established CC method for the hydrogen exchange reaction validated our approach and its implementation, and paved the way for its application to more challenging systems. As discussed earlier, the $N(^2D)+H_2$ reaction is considerably more demanding numerically than the $H+H_2$ system because the deep (~5.5 eV) NH_2 well requires a much larger basis and substantially longer propagation. To this end, the size of the wave packet ($J=0$) is approximately 1.6 million and the number of the propagation steps is 10 000. So far, DCSs for this reaction have only been computed using a time-independent method [61–63], while wave-packet calculations have been restricted to the total reaction probability [35,65,66]. To the best of our knowledge, this is the first report of exact quantum state-to-state DCSs for this reaction using a wave-packet method.

The results reported here were obtained using the potential energy surface of Ho *et al.* [67], which is more accurate than the one used by previous time-independent work [61–63]. Fully Coriolis-coupled wave packets up to $J=15$ were propagated for 10 000 steps, which enabled us to calculate DCSs up to the collision energy of about 0.085 eV. More extensive results, which require S matrices at higher J values, will be published later.

In Fig. 4, the vibrationally resolved and total DCSs for the $N+H_2(v_i=j_i=0)$ reaction at a collision energy of 0.082 66 eV are displayed. As the figure shows, the product angular distributions are dominated by scattering in both the backward and forward directions, indicative of a significant time delay in the scattering. The bias towards the backward scattering angles, particularly in the low-lying vibrational channels, is an indication that the reaction is not entirely statistical. This point has been realized before, and was attributed to the large exothermicity which results in a relatively short lifetime for the NH_2 complex [60,63,68]. Indeed, our recent results on the total reaction probabilities showed relatively broad peaks, signifying the participation of short-lived resonances [35].

The DCSs in Fig. 4 clearly indicate that the product vibrational distribution decays monotonically with the vibrational quantum number (v_f). This is also consistent with the previous theoretical work and can be attributed to the complex-forming reaction mechanism [61–63,69].

The rovibrationally resolved integral cross sections for the same reaction are given in Fig. 5, again at 0.08 266 eV. The product rotational distributions are all inverted and extend to the largest possible rotational levels allowed by the available

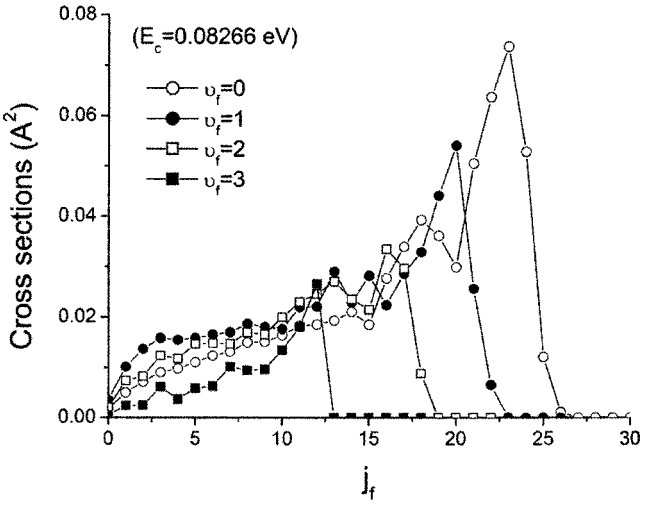

FIG. 5. Rovibrational state-resolved integral cross sections for the $N+H_2(v_i=j_i=0)\rightarrow NH+H$ reaction at 0.08 266 eV.

energy. Again, these distributions are also consistent with previous quantum mechanical results [61–63,69] and reflect the near-statistical nature of the reaction.

IV. CONCLUSIONS

In this work, an accurate and efficient wave-packet method based on the Chebyshev propagation is introduced for calculating quantum state-to-state differential and integral cross sections for atom-diatom reactive scattering. Like other wave-packet based methods, this approach generates a column of the S matrix in an energy range, and has favorable scaling laws in both memory and CPU. The Chebyshev propagation has the additional advantage that it can be accurately and efficiently carried out using the Chebyshev recursion formula and in real arithmetic. This method is tested with the benchmark $H+H_2$ reaction system by comparing with time-independent coupled-channel results and further applied to a more difficult system, namely the $N(^2D)+H_2$ insertion reaction. The implementation in the Open MP environment allows linear scaling with respect to the nodes in a shared memory computer, resulting in a significant reduction of the elapse time needed for such intensive calculations. Finally, we note that this wave-packet method can be readily generalized to polyatomic reactive scattering systems.

ACKNOWLEDGMENTS

This work was supported by the National Science Foundation (Grant No. CHE-0348858) and the Department of Energy (Grant No. DE-FG02-05ER15694). S.Y.L. thanks Professor D. Xie for some useful discussions.

[1] P. Casavecchia, Rep. Prog. Phys. **63**, 355 (2000).
[2] K. Liu, Annu. Rev. Phys. Chem. **52**, 139 (2001).
[3] F. Fernandez-Alonso and R. N. Zare, Annu. Rev. Phys. Chem. **53**, 67 (2002).
[4] R. T. Skodje and X. Yang, Int. Rev. Phys. Chem. **23**, 253 (2004).
[5] S. C. Althorpe, F. Fernandez-Alonso, B. D. Bean, J. D. Ayes, A. E. Pomerantz, R. N. Zare, and E. Wrede, Nature (London) **416**, 67 (2002).
[6] S. Harich, D. X. Dai, C. C. Wang, X. Yang, S. D. Chao, and R. T. Skodje, Nature (London) **419**, 281 (2002).
[7] D. X. Dai, C. C. Wang, S. Harich, X. Y. Wang, X. Yang, S. D. Chao, and R. T. Skodje, Science **300**, 1730 (2003).
[8] M. Qiu, Z. Ren, L. Che, D. X. Dai, S. Harich, X. Wang, X. Yang, C. Xu, D. Xie, M. Gustafasson, R. T. Skodje, Z. Sun, and D. H. Zhang, Science **311**, 1440 (2006).
[9] G. C. Schatz and A. Kuppermann, J. Chem. Phys. **65**, 4642 (1976).
[10] G. C. Schatz, J. Chem. Phys. **100**, 12839 (1996).
[11] J. Z. H. Zhang, *Theory and Application of Quantum Molecular Dynamics* (World Scientific, Singapore, 1999).
[12] S. C. Althorpe and D. C. Clary, Annu. Rev. Phys. Chem. **54**, 493 (2003).
[13] R. T. Pack and G. A. Parker, J. Chem. Phys. **87**, 3888 (1987).
[14] J. Z. H. Zhang and W. H. Miller, J. Chem. Phys. **91**, 1528 (1989).
[15] D. Skouteris, J. F. Castillo, and D. E. Manolopoulos, Comput. Phys. Commun. **133**, 128 (2000).
[16] Y. Sun, R. C. Mowrey, and D. J. Kouri, J. Chem. Phys. **87**, 339 (1987).
[17] D. Neuhauser, M. Baer, R. S. Judson, and D. J. Kouri, J. Chem. Phys. **93**, 312 (1990).
[18] D. H. Zhang and J. Z. H. Zhang, J. Chem. Phys. **101**, 1146 (1994).
[19] A. J. H. M. Meijer and E. M. Goldfield, J. Chem. Phys. **108**, 5404 (1998).
[20] W. H. Miller and Z. H. J. Zhang, J. Chem. Phys. **95**, 12 (1991).
[21] J. Dai and J. Z. H. Zhang, J. Chem. Phys. **100**, 6898 (1996).
[22] S. C. Althorpe, J. Chem. Phys. **114**, 1601 (2001).
[23] K. Yuan, Y. Cheng, X. Liu, S. Harich, X. Yang, and D. H. Zhang, Phys. Rev. Lett. **96**, 103202 (2006).
[24] H. Tal-Ezer and R. Kosloff, J. Chem. Phys. **81**, 3967 (1984).
[25] B. Hartke, R. Kosloff, and S. Ruhman, Chem. Phys. Lett. **158**, 96 (1986).
[26] Y. Huang, W. Zhu, D. J. Kouri, and D. K. Hoffman, Chem. Phys. Lett. **206**, 96 (1993).
[27] Y. Huang, W. Zhu, D. J. Kouri, and D. K. Hoffman, Chem. Phys. Lett. **214**, 451 (1993).
[28] Y. Huang, D. J. Kouri, and D. K. Hoffman, Chem. Phys. Lett. **225**, 37 (1994).
[29] Y. Huang, D. J. Kouri, and D. K. Hoffman, J. Chem. Phys. **101**, 10493 (1994).
[30] R. Chen and H. Guo, J. Chem. Phys. **105**, 3569 (1996).
[31] S. K. Gray and G. G. Balint-Kurti, J. Chem. Phys. **108**, 950 (1998).
[32] S. Y. Lin and H. Guo, J. Chem. Phys. **117**, 5183 (2002).
[33] S. Y. Lin and H. Guo, J. Chem. Phys. **119**, 11602 (2003).
[34] S. Y. Lin and H. Guo, J. Phys. Chem. A **108**, 2141 (2004).
[35] S. Y. Lin and H. Guo, J. Chem. Phys. **124**, 031101 (2006).
[36] S. C. Althorpe, D. J. Kouri, D. K. Hoffman, and J. Z. H. Zhang, J. Chem. Soc., Faraday Trans. **93**, 703 (1997).
[37] S. C. Althorpe, D. J. Kouri, and D. K. Hoffman, J. Chem. Phys. **106**, 7629 (1997).
[38] J. C. Light and T. Carrington Jr., Adv. Chem. Phys. **114**, 263 (2000).
[39] R. Kosloff, in *Numerical Grid Methods and Their Applications to Schrodinger's Equation*, edited by C. Cerjan (Kluwer, Dordrecht, 1993).
[40] E. U. Condon and G. H. Shortley, *The Theory of Atomic Spectra* (Cambridge, London, 1964).
[41] R. N. Zare, *Angular Momentum* (Wiley, New York, 1988).
[42] G. C. Corey and D. Lemoine, J. Chem. Phys. **97**, 4115 (1992).
[43] G. C. Corey and J. W. Tromp, J. Chem. Phys. **103**, 1812 (1995).
[44] G. G. Balint-Kurti, Adv. Chem. Phys. **128**, 249 (2004).
[45] V. A. Mandelshtam and H. S. Taylor, J. Chem. Phys. **102**, 7390 (1995).

[46] V. A. Mandelshtam and H. S. Taylor, J. Chem. Phys. **103**, 2903 (1995).
[47] D. Neuhauser and M. Baer, J. Chem. Phys. **90**, 4351 (1989).
[48] H. Guo, in *Theory of Chemical Reaction Dynamics*, edited by A. Lagana and G. Lendvay (Kluwer, Dordrecht, 2004), p. 217.
[49] R. Chen and H. Guo, J. Chem. Phys. **108**, 6068 (1998).
[50] G. C. Corey, J. W. Tromp, and D. Lemoine, in *Numerical Grid Methods and Their Applications to Schroedinger's Equation*, edited by C. Cerjan (Kluwer, Dordrecht, 1993), p. 1.
[51] D. J. Tannor and D. E. Weeks, J. Chem. Phys. **98**, 3884 (1993).
[52] D. J. Kouri, Y. Huang, W. Zhu, and D. K. Hoffman, J. Chem. Phys. **100**, 3662 (1994).
[53] T. Seideman and W. H. Miller, J. Chem. Phys. **96**, 4412 (1992).
[54] R. S. Judson, D. J. Kouri, D. Neuhauser, and M. Baer, Phys. Rev. A **42**, 351 (1990).
[55] F. Gogtas, G. G. Balint-Kurti, and A. R. Offer, J. Chem. Phys. **104**, 7927 (1996).
[56] T. Peng and J. Z. H. Zhang, J. Chem. Phys. **105**, 6072 (1996).
[57] D. J. Kouri, D. K. Hoffman, T. Peng, and J. Z. H. Zhang, Chem. Phys. Lett. **262**, 519 (1996).
[58] S. C. Althorpe, D. J. Kouri, and D. K. Hoffman, J. Phys. Chem. A **102**, 9494 (1998).
[59] A. Messiah, *Quantum Mechanics* (Wiley, New York, 1968).
[60] E. J. Rackham, T. Gonzalez-Lezana, and D. E. Manolopoulos, J. Chem. Phys. **119**, 12895 (2003).
[61] P. Honvault and J.-M. Launay, J. Chem. Phys. **111**, 6665 (1999).
[62] N. Balucani, L. Cartechini, G. Capozza, E. Segoloni, P. Casavecchia, G. Gualberto Volpi, F. J. Aoiz, L. Banares, P. Honvault, and J.-M. Launay, Phys. Rev. Lett. **89**, 013201 (2002).
[63] N. Balucani, P. Casavecchia, L. Banares, F. J. Aoiz, T. Gonzalez-Lezana, P. Honvault, and J.-M. Launay, J. Phys. Chem. A **110**, 817 (2006).
[64] A. I. Boothroyd, W. J. Keogh, P. G. Martin, and M. R. Peterson, J. Chem. Phys. **104**, 7139 (1996).
[65] P. Defazio and C. Petrongolo, J. Theor. Comput. Chem. **2**, 547 (2003).
[66] T.-S. Chu, K.-L. Han, and A. J. C. Varandas, J. Phys. Chem. A **110**, 1666 (2006).
[67] T.-S. Ho, H. Rabitz, F. J. Aoiz, L. Banares, S. A. Vazquez, and L. B. Harding, J. Chem. Phys. **119**, 3063 (2003).
[68] L. Banares, F. J. Aoiz, T. Gonzalez-Lezana, V. J. Herrero, and I. Tanarro, J. Chem. Phys. **123**, 224301 (2005).
[69] E. J. Rackham, F. Huarte-Larranaga, and D. E. Manolopoulos, Chem. Phys. Lett. **343**, 356 (2001).